New Journal of Chemistry

N-doped carbon nanospheres with nanocavities to encapsulate manganese oxides toward ORR electrocatalysts

Minggui Wang,[a,b] Fang Peng,[a] Min Wang,[a] Jie Han[*b]

[a] Guangling College, Yangzhou University, Yangzhou, Jiangsu 225009, P. R. China

[b] School of Chemistry and Chemical Engineering, Yangzhou University, Yangzhou, Jiangsu 225002, P. R. China

List of supplementary material

SI-1 Details for electrochemical test.

Fig. S1 (a) Raman spectra and (b) XPS survey spectrum of N-CN@MnO$_2$ hybrids, XPS spectra of (c) C 1s, (d) N 1s and (e) Mn 2p of N-CN@MnO$_2$ hybrids, (f) XRD pattern of N-CN@MnO$_2$ hybrids.

Fig. S2 XPS spectra of (a) C 1s and (b) N 1s for N-CN@Mn$_3$O$_4$, (c) C 1s and (d) N 1s for N-CN@MnO.

Fig. S3 Relative ratios of various nitrogen types in N-CN@MnO$_2$, N-CN@Mn$_3$O$_4$ and N-CN@MnO hybrids.

Fig. S4 Cycle voltammetry curves of (a) N-CNs, (b) N-CN@MnO$_2$, (c) N-CN@Mn$_3$O$_4$, (d) N-CN@MnO hybrids and (e) Pt/C in N$_2$- and O$_2$-saturated 0.1 M KOH with a scan rate of 20 mV s^{-1}.

Fig. S5 LSV curves of (a) N-CNs, (b) N-CN@MnO$_2$, (c) N-CN@MnO hybrids and (d) Pt/C in O$_2$-saturated 0.1 M KOH with various rotating speeds.

Fig. S6 (a) The differential plots of I versus E constructed from the LSV curve. (b) K-L plots of N-CN@Mn$_3$O$_4$ at 0.3-0.5 V. (c) Peroxide yield (solid line) and the electron transfer number (dotted line) of different catalysts at different potentials.

Fig. S7 SEM images of N-CN@Mn$_3$O$_4$ hybrids (a) before and (b) after long-term stability testing, (c) XRD patterns of N-CN@Mn$_3$O$_4$ before and after catalytic reaction.

Table S1 BET surface area and BJH pore size and volume of N-CN@MnO$_2$, N-CN@Mn$_3$O$_4$ and N-CN@MnO hybrids.

Table S2 Comparison of the electrochemical performances of N-CN@Mn$_3$O$_4$ sample involved in ORR with reported results. References

Electrochemical test

Electrochemical measurements including cyclic voltammetry (CV), linear scan voltammogram (LSV) and stability were performed on an electrochemical workstation (VMP3, Biologic, France) equipped with a three-electrode cell system. A rotating ring-disk electrode (RRDE) of 5.61 mm in disk diameter loaded with electrocatalyst was used as the working electrode with Ag/AgCl electrode as the reference electrode, and Pt wire as the counter electrode. The oxygen reduction reaction was carried out in an O_2 saturated 0.1 M KOH aqueous solution. The stability test was collected at 0.8 V vs. Ag/AgCl with a rotation speed of 400 rpm.

The working electrode was prepared as follows: 10.0 mg of catalyst were dispersed in solvent mixture of 5 wt % Nafion solution (0.05 mL) and 2-propanol (0.95 mL) under sonication for 1 h to form a homogeneous ink. Then 7 μL of the resulting suspension was dropped onto a pre-polished rotating disk electrode (RRDE, $S_{disk} = 0.2475$ cm^2) and dried at room temperature. For comparison, commercial Pt/C-20% electrocatalyst (Sigma-Aldrich) was used.

The number of electrons transferred onto the as-prepared catalyst was calculated according to the Koutecky-Levich equation:

$$\frac{1}{J} = \frac{1}{J_L} + \frac{1}{J_K} = \frac{1}{B\omega^{\frac{1}{2}}} + \frac{1}{J_K} \tag{1}$$

Where J is the measured current, J_K is the kinetic current, ω is the electro rotating rate. B is determined from the slope of the Koutecky-Levich (K-L) plots according to the Levich equation as given below:

$$B = 0.62nFC_0(D_0)^{2/3}v^{-1/6} \tag{2}$$

where n represents the overall number of electrons transferred in oxygen reduction, F is the Faraday constant (96485 C mol^{-1}), C_0 is the bulk concentration of O_2 (1.2 × 10^{-6} mol cm^{-3}), D_0 is the diffusion coefficient of O_2 in 0.1 mol L^{-1} KOH electrolyte (1.9 × 10^{-5} cm^2 s^{-1}), v is the kinematic viscosity of the electrolyte (0.01 cm^2 s^{-1}).

The H_2O_2 yield and electron transfer number were calculated from the following

equation:

$$H_2O_2 \ (\%) = 200I_r / (NI_d + I_r) \qquad (3)$$

$$n = 4I_d / (I_d + I_r/N) \qquad (4)$$

where I_d and I_r are the disk and ring currents, respectively, and N is the current collection efficiency of RRDE. N was determined to be 0.37.

For the Tafel plot, the kinetic current was calculated from the mass-transport correction of RDE by:
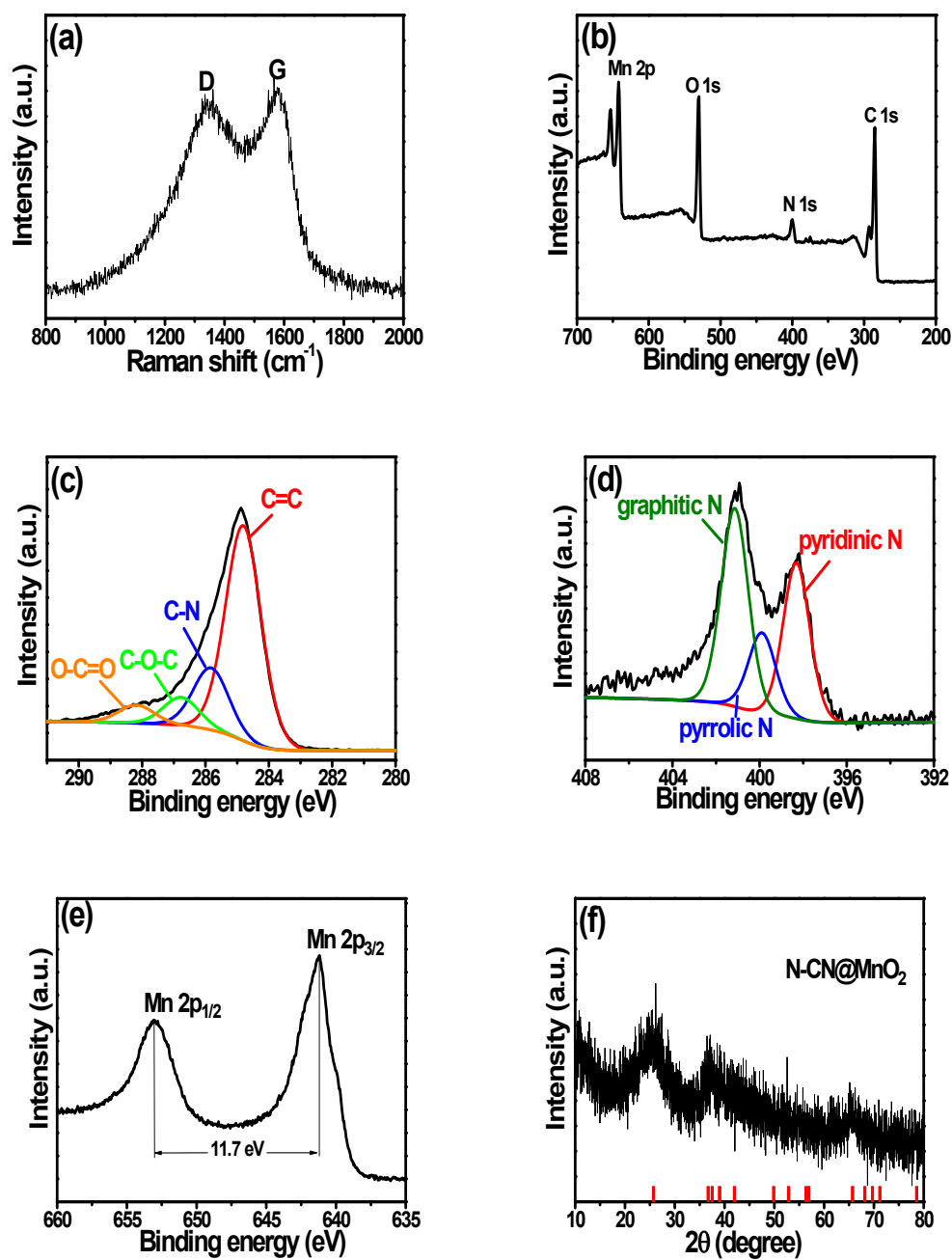
$$J_K = \frac{J * J_L}{J_L - J} \qquad (5)$$

Fig. S1 (a) Raman spectra and (b) XPS survey spectrum of N-CN@MnO$_2$ hybrids, XPS spectra of (c) C 1s, (d) N 1s and (e) Mn 2p of N-CN@MnO$_2$ hybrids, (f) XRD pattern of N-CN@MnO$_2$ hybrids.
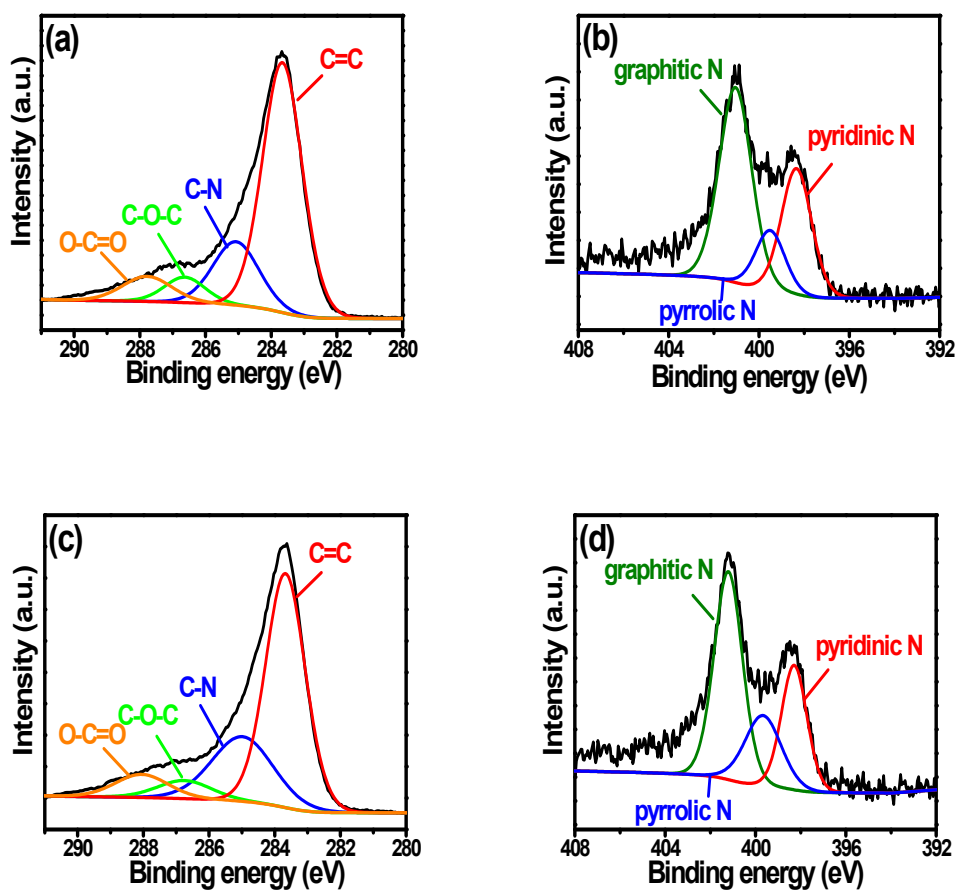
Fig. S2 XPS spectra of (a) C 1s and (b) N 1s for N-CN@Mn$_3$O$_4$, (c) C 1s and (d) N 1s for N-CN@MnO.
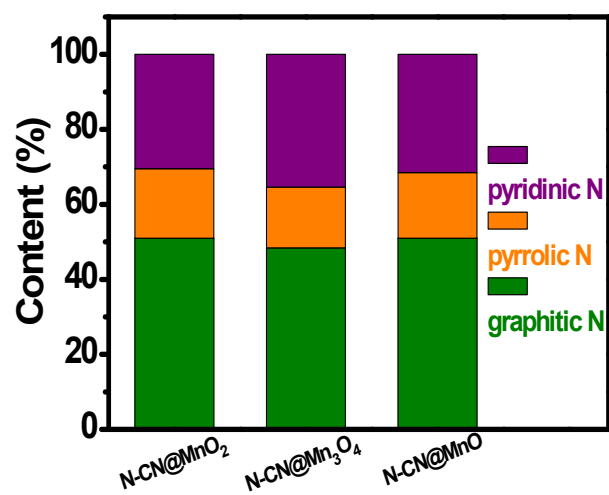
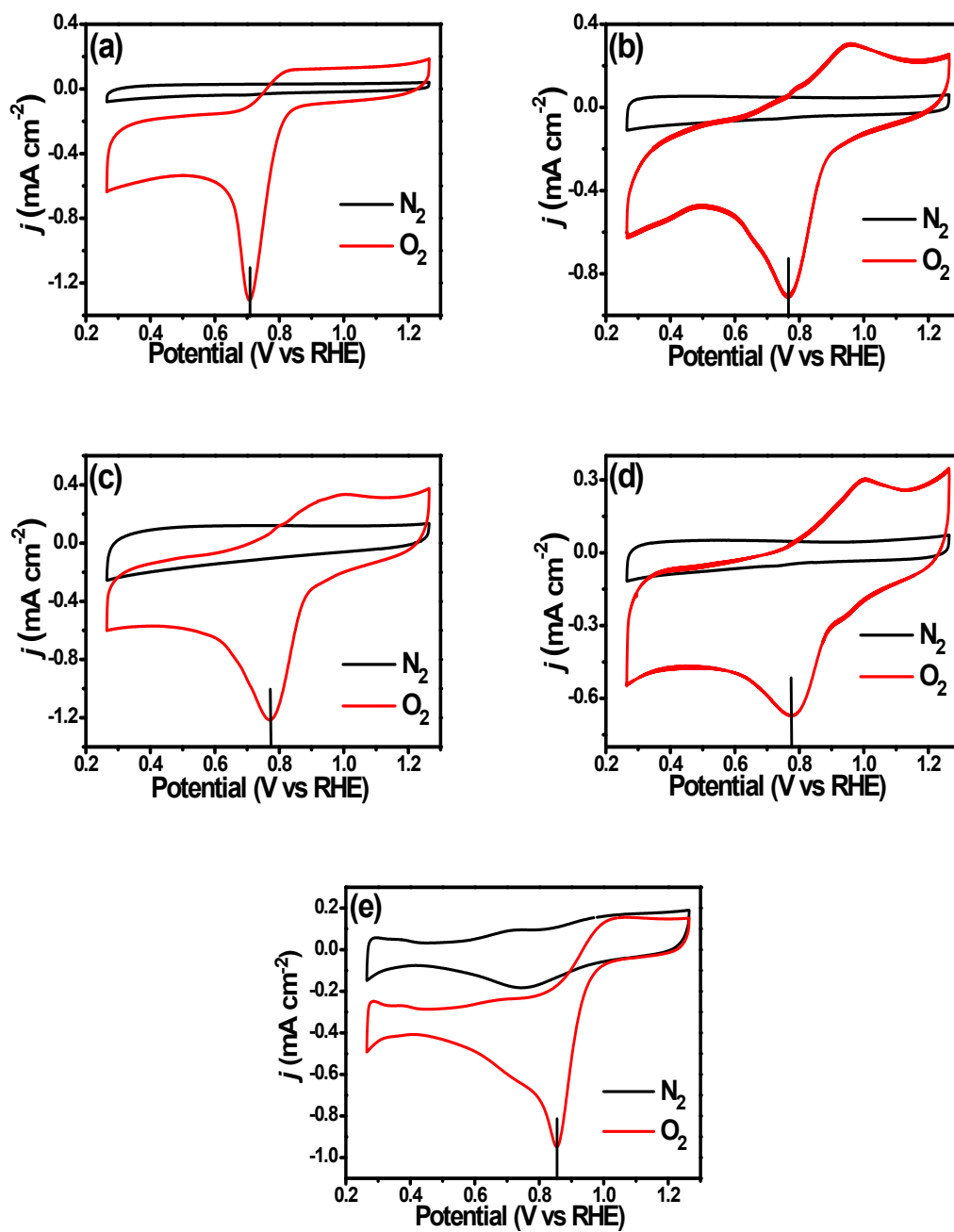**Fig. S3** Relative ratios of various nitrogen types in N-CN@MnO$_2$, N-CN@Mn$_3$O$_4$ and N-CN@MnO hybrids.

Fig. S4 Cycle voltammetry curves of (a) N-CNs, (b) N-CN@MnO$_2$, (c) N-CN@Mn$_3$O$_4$, (d) N-CN@MnO hybrids and (e) Pt/C in N$_2$- and O$_2$-saturated 0.1 M KOH with a scan rate of 20 mV s^{-1}.
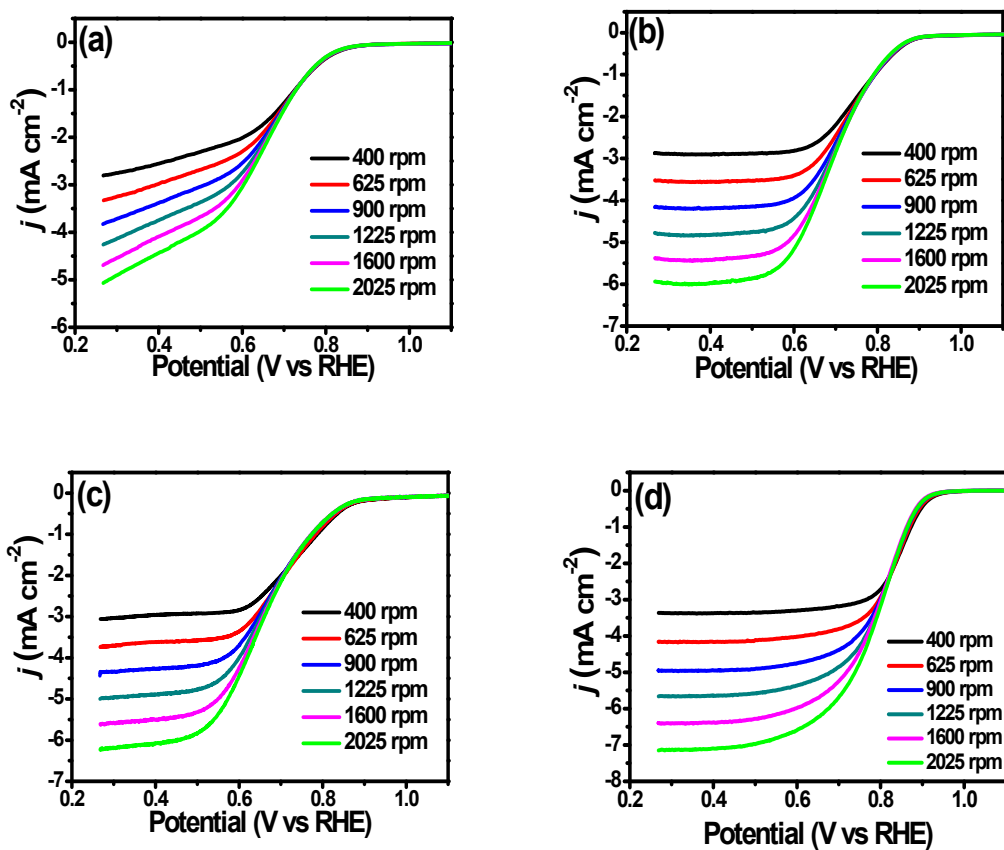
Fig. S5 LSV curves of (a) N-CNs, (b) N-CN@MnO₂, (c) N-CN@MnO hybrids and (d) Pt/C in O₂-saturated 0.1 M KOH with various rotating speeds.
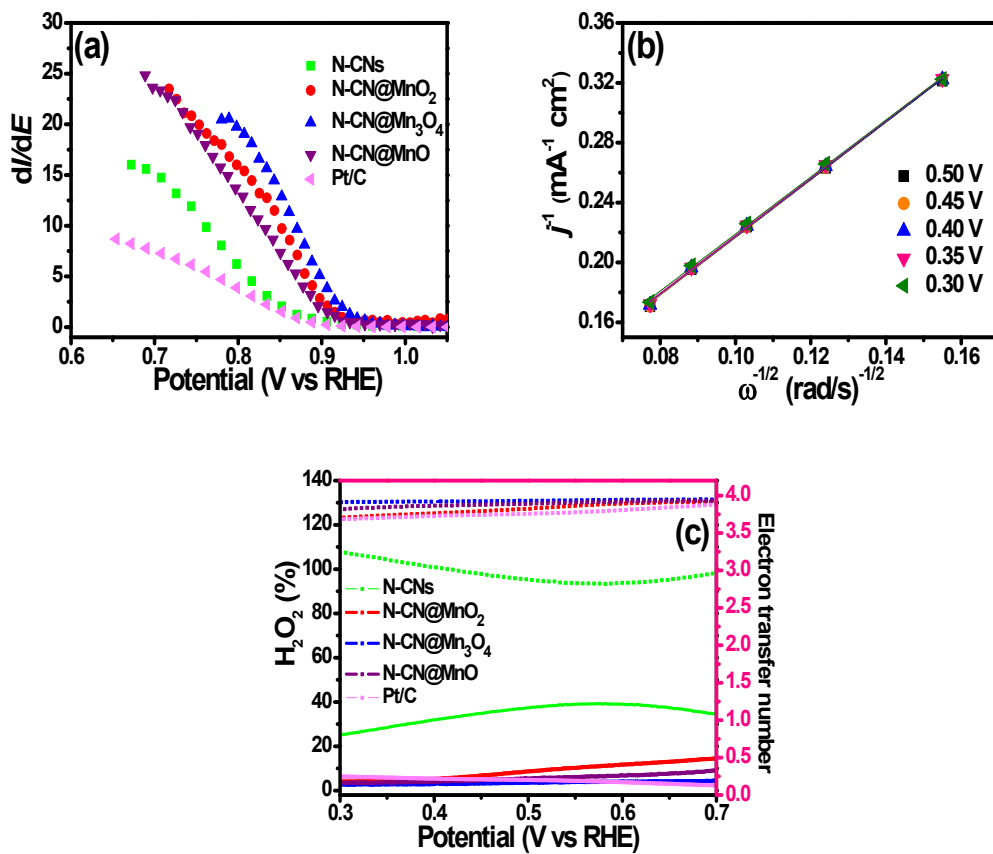
Fig. S6 (a) The differential plots of *I* versus *E* constructed from the LSV curve. (b) K-L plots of N-CN@Mn$_3$O$_4$ at 0.3-0.5 V. (c) Peroxide yield (solid line) and the electron transfer number (dotted line) of different catalysts at different potentials.
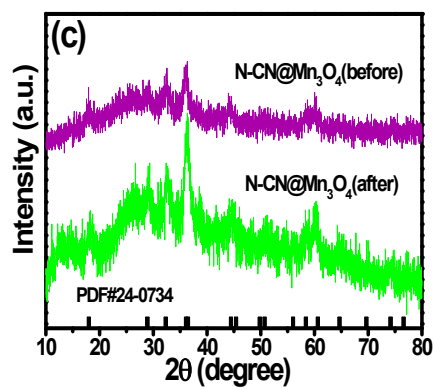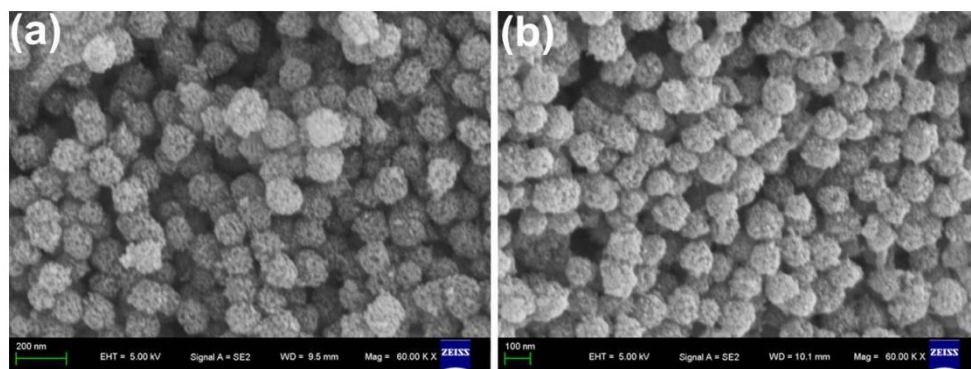
Fig. S7 SEM images of N-CN@Mn$_3$O$_4$ hybrids (a) before and (b) after long-term stability testing, (c) XRD patterns of N-CN@Mn$_3$O$_4$ before and after catalytic reaction.

Table S1 BET surface area and BJH pore size and volume of N-CN@MnO$_2$, N-CN@Mn$_3$O$_4$ and N-CN@MnO hybrids.

Catalyst	SSA (m^2 g^{-1})	TPV (cm^3 g^{-1})	Pore size (nm)
N-CN@MnO$_2$	244.1	0.5348	3.69
N-CN@Mn$_3$O$_4$	293.5	0.7451	3.71
N-CN@MnO	216.8	0.4546	10.6

Table S2 Comparison of the electrochemical performances of N-CN@Mn$_3$O$_4$ sample involved in ORR with reported results.

Catalyst	E_{onset} (V)	I_{s} (mA cm^{-2})	n	Reference
Mn$_3$O$_4$@GF_O$_3$	0.82	-2.8	3.8	1
Mn$_3$O$_4$/NCP	0.92	-5.24	3.91	2
graphene@Mn$_3$O$_4$	0.89	-5.85	3.91	3
Mn$_3$O$_4$/rGO	-	-4.37	3.81	4
Mn$_3$O$_4$/MXene	0.89	-3.15	3.4	5
g-C$_3$N$_4$@MWCNTs/Mn$_3$O$_4$	0.821	-4.47	3.80	6
N-CN@Mn$_3$O$_4$	0.906	-5.85	3.93	this work

References

1. M. P. Araújo, M. Nunes, I. M. Rocha, M. F. R. Pereira and C. Freire, *J. Mater. Sci.*, 2019, **54**, 8919-8940.

2. T. Najam, X. K. Cai, M. K. Aslam, M. K. Tufail and S. S. A. Shah, Int. *J. Hydrogen Energ.*, 2020, **45**, 12903-12910.

3. T. Wang, Q J. Le, X. L. Guo, M. Huang, X. Y. Liu, F. Dong, J. T. Zhang and Y. X. Zhang, *ACS Sustainable Chem. Eng.*, 2019, **7**, 831-837.

4. Y. Zhang, X. F. Zhang, M. R. Liu, Y. Q. Liu, H. D. Huang and S. Lin, *J. Solid State Electrchem.*, 2018, **22**, 2159-2168.

5. Q. Xue, Z. X. Pei, Y. Huang, M. S. Zhu, Z. J. Tang, H. F. Li, Y. Huang, N. Li, H. Y. Zhang and C. Y. Zhi, *J. Mater. Chem. A*, 2017, **5**, 20818-20823.

6. G. H. Li, T. Sun, Y. Fu, L. X. Lei and O. Zhuo, *J. Solid State Electrochem.*, 2016, **20**, 2685-2692.